The Rheology of a Concentrated Colloidal Suspension of Hard Spheres

D. ANDREW R. JONES,* BRUCE LEARY,† AND DAVID V. BOGER*,[1]

*Department of Chemical Engineering, University of Melbourne, Parkville, Victoria 3052, Australia, and †Dulux Australia, Clayton, Victoria, Australia

Received December 31, 1990; accepted April 29, 1991

The rheology of a model hard-sphere suspension has been studied at high volume fraction. Particular emphasis was placed on observing the transition between liquid-like and solid-like behavior at the maximum packing volume fraction. Capillary viscometry has shown that the suspension viscosity at low concentration agrees well with theory and other experimental work on hard-sphere systems. At higher concentrations the rheological properties, measured using steady shear, oscillatory shear, and creep techniques, change rapidly from viscous Newtonian to shear-thinning viscoelastic. When the volume fraction is greater than the maximum packing volume fraction the behavior is like that of an elastic solid, and a yield stress can be measured using cone and plate instruments and the vane method. At high volume fractions the product of a characteristic shear rate (or Peclet number) and the low shear limiting viscosity is found to be almost independent of concentration. It is possible to superimpose all the steady shear data using a scaling based on the Cross equation.

INTRODUCTION

In recent years, interest in the rheology of suspensions has greatly increased. In particular, attempts have been made to measure the rheological properties of stable, well-characterized model systems (1–7) and to determine their microstructure under shear using scattering techniques (8–12). Theories (13–17) and computer simulations (18–23) have shed light on these properties but a full understanding is still restricted to low concentrations. The aim of this work is to extend the rheological study of model hard-sphere suspensions to high concentrations using a variety of rheological techniques including steady shear, oscillatory shear, and creep experiments.

Very few colloidal suspensions closely resemble hard spheres in their behavior, i.e., exhibit no interparticle interaction until contact when there is an infinite repulsion. The most studied example is the hydrophobic silica developed by Vrij and co-workers (24–27), which consists of monodisperse silica particles coated with a dense layer of stearyl alcohol ($C_{18}H_{37}OH$) dispersed in cyclohexane. An extensive series of studies by light-scattering (25), small-angle X-ray scattering (26), and small-angle neutron scattering (SANS) (27) has shown that these particles behave as hard spheres up to quite high concentrations.

Recently, steady shear experiments have been conducted on this system (1–3) over a wide range of concentration (volume fraction, ϕ, up to 0.6), shear rate, and particle size. The following trends were observed. At low concentrations the suspensions are Newtonian and the viscosity is predicted fairly well by the theoretical expressions of Einstein (13) and Batchelor (14). At moderate concentrations ($0.2 < \phi < 0.3$) the viscosity increases more rapidly but no shear thinning is observed. Above $\phi = 0.3$, a Newtonian plateau is found in the viscosity at low and high shear rates, separated by a shear thinning region. The viscosity rises very rapidly as ϕ approaches the maximum packing volume fraction, $\phi_m \cdot \phi_m = 0.63$ at low shear rate and 0.71 at high shear

[1] To whom all correspondence should be addressed.

0021-9797/91 $3.00

rate. The high concentration results ($0.3 < \phi < 0.6$) are modeled well by Quemada's expression (28)

$$\eta_r = \left(1 - \frac{\phi}{\phi_m}\right)^{-2}, \quad [1]$$

where the relative viscosity $\eta_r = \eta/\eta_s$, η_s being the solvent viscosity. The above equation is similar to that of Krieger and Dougherty (29) which could also be used. It was also found that the effects of size could be scaled using a reduced shear stress or Peclet number,

$$P_e = \eta_s \dot{\gamma} \frac{a^3}{kT}, \quad [2]$$

where $\dot{\gamma}$ is the shear rate and a is the particle radius. Thus, as particle size increases, the shear thinning region shifts to lower shear rates. In addition, no shear thickening or yield stress was observed. Oscillatory shear experiments on similar suspensions (4, 5) were used to measure the viscoelastic properties at high frequency (80–200 kHz). The data were characterized by a relaxation time which increased rapidly as concentration increased. It was concluded that the viscoelasticity is due to Brownian forces restoring the suspension structure.

The other hard-sphere colloidal suspension that has been systematically studied is poly(methyl methacrylate) (PMMA) particles dispersed in a hydrocarbon medium. The particles are sterically stabilized by poly(hydroxystearic acid). For larger particles ($a > 200$ nm) the steric repulsion approximates to a hard-sphere interaction. Steady and oscillatory shear studies on these suspensions (6, 7) show trends similar to those on the silica systems, but in addition apparent yield stress behavior was observed at high concentration ($\phi > 0.6$) as was shear thickening under certain conditions at high shear rates.

There have been numerous studies on model soft-sphere suspensions, the "soft" interaction being due to an adsorbed polymer layer or an electrostatic double layer. Mewis (30) has reviewed the rheology of polymerically stabilized suspensions which together with some more recent work (31, 32) suggests that these systems have properties very similar to those of hard spheres except at high concentrations when the stabilizing layers interact or at high shear rates when the layers can be perturbed by the hydrodynamic forces. Charge stabilized suspensions have been widely studied (33–36) and exhibit quite different properties from hard spheres. The long-range electrostatic interaction can result in a crystal-like structure with a measurable yield stress occurring at relatively low concentrations. Elastic moduli determined by oscillatory experiments have been quite successfully modeled by theories based on the electrostatic interaction (34, 35).

Significant advances have been made in the understanding of suspension rheology through the study of the microstructure under shear using scattering techniques. Early light-scattering studies by Hoffman (8) showed that the microstructure changed as shear rate increased. More recent work on hard spheres using light scattering (10–12) and SANS (9) show that the structure is distorted even at low shear rates. However, there is still some ambiguity as to the type of structures formed at higher shear rates. Crystalline, layered, string-like, and amorphous structures have all been observed but it has not yet been clearly shown how these relate to the rheological properties.

Theoretical development has been hampered by the difficulty of calculating the many-body thermodynamic interactions (arising from Brownian motion and interparticle interactions) and the many-body hydrodynamic interactions which are important at moderate and high concentrations. Batchelor (14) laid the foundation for recent progress by calculating both contributions at low concentrations ($\phi < 0.2$) and thus extended Einstein's first-order equation (13) to

$$\eta_r = 1 + 2.5\phi + 6.2\phi^2 + O(\phi^3). \quad [3]$$

Russel and Gast (15) and Wagner and Russel (16) have extended Batchelor's work using a statistical mechanical approach to incorporate

the many-body thermodynamic contributions at high concentration while including the hydrodynamic interactions at a pairwise level. Beenakker (17) calculated the many-body hydrodynamic contribution for all concentrations but neglected Brownian forces. Each of these theories tends to underestimate the viscosity at high concentration ($\phi > 0.4$).

Recently two theories have attempted to describe specific aspects of hard-sphere suspension rheology. Dhont *et al.* (39) calculated the viscosity as a function of shear rate from a consideration of the shear-induced distortion of the microstructure, while Mellema *et al.* (40) described the viscoelastic behavior of a hard-sphere suspension using a model of statistical springs acting between the particles, from which a relaxation strength was calculated.

Computer simulations of suspension dynamics, although still fairly limited, have produced some interesting results. Studies (20, 21) have been made of various rheological properties including shear thinning and thickening but directly relating these to experimental data is difficult. Comparisons have been made between molecular dynamics simulations of simple fluids (18, 22, 23) and structural ordering observed in colloidal suspensions at high shear rates. The simulations have predicted the existence of layered and string-like structures.

This study extends the experimental data available in the literature on model hard-sphere suspensions. The steady shear rheology is investigated as a function of shear rate over a very wide range of concentrations up to and above the maximum packing volume fraction. Four different instruments are used and compared: an Ubbelohde capillary viscometer, a constant shear rate Rheogoniometer, and two constant stress instruments. The results are compared with other hard-sphere data and the low concentration theories. Relatively small particles are used ($a = 25$ nm), one advantage of which is that the behavior at low Peclet number is accessible. The viscoelastic properties at high concentration are studied using constant stress and constant shear rate instruments and change rapidly as ϕ approaches ϕ_m. When $\phi > \phi_m$, solid-like behavior is observed and the suspensions exhibit a yield stress. Finally, creep experiments show viscoelastic characteristics up to ϕ_m, while above ϕ_m solid-like behavior is again seen at low stress.

MATERIALS AND METHODS

A. Particle Preparation and Characterization

The silica particles were prepared using the method of Stöber *et al.* (41) in which tetraethylsiloxane (TES; BDH AnalaR grade) is added to a mixture of aqueous ammonia (BDH 30%, w/w) and ethanol (BDH AnalaR grade) under a nitrogen atmosphere and stirred for 24 h. The TES hydrolyzes, catalyzed by the ammonia, producing tetrahydroxysilane which polymerizes to form spherical particles. The final particle size is controlled by the concentrations of water and ammonia. The particles used in this study were prepared in a 5-liter batch. The reagent concentrations were TES, 0.2 mole/dm^3; NH_3 (aq), 0.725 mole/dm^3; and the balance made up with ethanol. The temperature was maintained at 30 ± 0.5°C using a water bath.

The particles were coated as described by van Helden *et al.* (24). This involved adding stearyl alcohol ($C_{18}H_{37}OH$) to the dispersion of charge-stabilized silica particles and distilling off the ethanol, water, and ammonia. The stearyl alcohol melt was then held at 180°C for 4 h and allowed to cool. The residue was dissolved in a cyclohexane/chloroform mixture and redispersed several times in cyclohexane by centrifugation.

The size distribution was determined from electron micrographs of the particles. A typical photograph is shown in Fig. 1. Nine hundred particles were counted, giving a mean diameter of 49 nm with a standard deviation of 6.5 nm. Figure 2 shows the size distribution. The surface area of the coated particles, determined using BET nitrogen adsorption, was 59 m^2/g, which is comparable with results from pre-

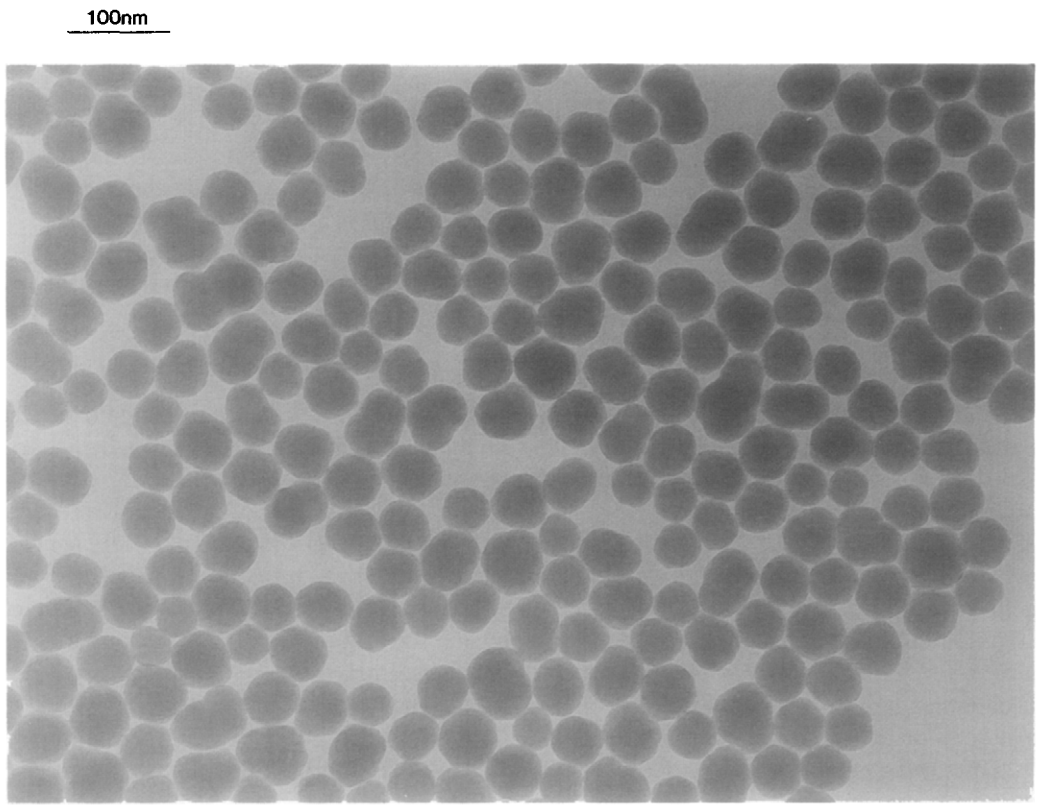

FIG. 1. Electron micrograph of coated silica.

vious work (24). Quantitative analyses for carbon and hydrogen were obtained giving 12.6 and 2.6%, w/w, respectively, which are again similar to other reported data and indicate that the particles are indeed coated with the stearyl chains.

Small-angle X-ray scattering experiments were performed in the Department of Chemistry at the Australian National University (42) on dilute (<1%, w/w) solutions of the silica in cyclohexane. Analysis of the data showed the particles to be acting as hard spheres and the diameter obtained by fitting a spherical form factor was 54 nm.

B. Sample Preparation

Most studies on stearyl-coated silica particles have used cyclohexane as the solvent because its refractive index (1.427) is close to that of the particles (1.438 (43)). It has been shown (44) that under these conditions the van der Waals attraction is minimized and the solvent's nonpolar nature suppresses the electrostatic interactions. The major problem with cyclohexane is its high volatility which causes

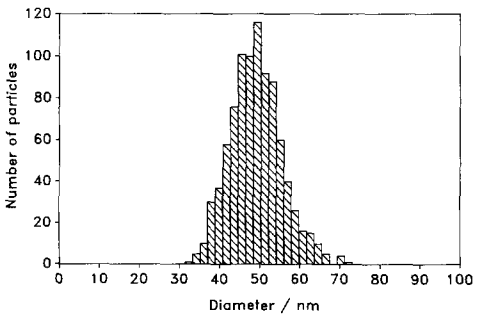

FIG. 2. Particle diameter distribution from electron microscopy.

difficulties when handling samples, especially at high concentration. Thus the particles in this work were dispersed in a high boiling hydrocarbon medium, Shellsol T from Shell Co. (bp = 186°C). This solvent is nonpolar and has a refractive index of 1.423, which is close to that of cyclohexane. The density was determined by picnometry to be 0.764 ± 0.001 g/ml and the viscosity determined using a Ubbelohde viscometer to be 1.38 ± 0.01 cP at 20 ± 0.05°C.

The dispersions in cyclohexane were filtered and then dried in a stream of dry air at room temperature and placed in an oven at 90°C for 1 h. Samples of specific concentration were made up gravimetrically using a four-figure balance in glass screw top bottles. Those samples which would flow were mixed by turning end over end for several hours or days depending on the concentration. Nonflowing samples were stirred manually and reweighed to monitor any change in concentration. Any trapped air bubbles in these samples were removed by gentle centrifugation. The accuracy of the weight concentration of the samples was better then 0.1%. The fact that the dried particles spontaneously redispersed in solvent indicates that there is no significant van der Waals attraction between them.

Samples at all concentrations were perfectly transparent, indicating a good refractive index match with the solvent. A slight yellow coloration appeared during the coating reaction which was presumably due to slight charring of the stearyl alcohol.

C. Rheological Tests

An Ubbelohde capillary viscometer was used to determine the intrinsic viscosity of the silica suspension at low concentration. This has been shown (2, 6) to be an effective method of determining the specific volume of suspensions. The following procedure was employed. The viscometer was placed in a water bath and the temperature maintained at 20.0 ± 0.1°C. Shellsol T was placed in the viscometer and the time measured for a set volume to flow through the capillary. This was repeated at least 10 times, the typical time being about 200 s. The viscometer was then removed from the bath and weighed, and then a weighed amount of stock suspension was added. This enabled the concentration of the test fluid to be accurately determined. The viscometer was returned to the bath and the temperature allowed to equilibrate before the next set of timings was made. Samples of up to 2% (w/w) were tested. Evaporation of the solvent was not detectable by weight over a period of several hours. A capillary of 0.35 mm diameter was used, giving a maximum shear rate of approximately 700/s. A series of experiments was conducted at higher concentrations using a similar procedure.

Three cone and plate instruments were used to study higher concentration solutions. The first was an R19 Weissenberg rheogoniometer with a cone of 75 mm diameter and 2.47° angle. The accessible shear rate range was 0.002–1000 s^{-1} and the oscillation frequency range was 0.01–20 Hz. The machine was operated manually but data collection and analysis were performed using a microcomputer. Sample temperature was controlled to within 0.1°C using an oil-filled jacket. Steady and oscillatory shear tests were conducted on each sample. The instrument also has the facility to measure normal stresses. In the oscillatory mode, measurements were made as a function of strain amplitude (γ_0) to check for linearity, i.e., the region of low γ in which the viscoelastic parameters are independent of γ_0. Studies (6) have shown that the linear region for suspensions is much more limited than that for polymeric systems. Measurements were performed using a γ_0 well within the linear region, typically $\gamma_0 \sim 0.008$. Finally the steady shear behavior was tested again to check for any drying effects. Each sample was in the rheometer for about 40 min, over which time no change in the rheological properties was detected.

A Bohlin constant stress instrument was used with a cone of 40 mm diameter and 4° angle. This had the advantage of requiring

smaller samples than the Weissenberg. Both operation and data analysis were carried out by a microcomputer. This rheometer could be programmed to take readings at a series of increasing/decreasing applied stresses or to measure the dynamic properties for a series of oscillation frequencies at a set stress. It also had a creep facility which would monitor the strain as a function of time for a set applied stress. A water bath controlled the temperature to within 0.1°C.

The third instrument was a Carri-Med constant stress device which has the same features as the Bohlin machine but in addition could be programmed to do a stress sweep experiment in which the applied stress was smoothly increased over a set time period. Also the dynamic experiment could be conducted at constant strain amplitude as well as constant stress, which is valuable for suspensions with their limited linearity. The temperature was controlled by a Peltier mechanism to within 0.1°C. One advantage of the Carri-Med was the availability of a solvent trap which, when filled with water, would reduce evaporation considerably, allowing a sample to be left in the machine for several hours with no appreciable change in properties.

The final rheological technique was yield stress, σ_y, measurement using the vane method developed at Melbourne University (45), which overcomes the problem of wall slip and gives a one-point determination of σ_y avoiding extrapolations from steady shear data. The vane consists of four thin blades arranged at equal angles around a small cylindrical shaft. This assembly is attached to a Haake constant shear rate rheometer. The vane is immersed in the sample and the torque growth monitored as it is slowly rotated. The yield stress is calculated from the maximum torque recorded.

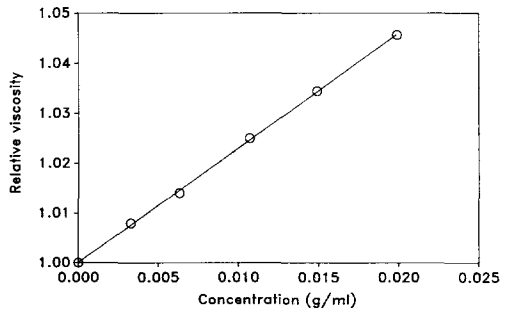

FIG. 3. Specific volume from Ubbelohde viscometry.

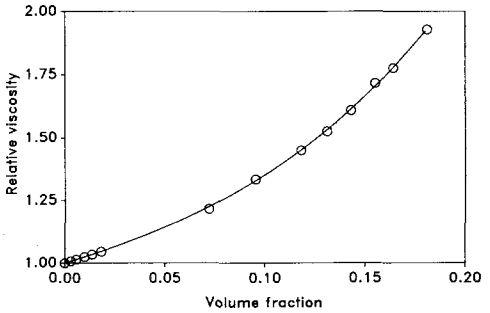

FIG. 4. Ubbelohde viscometry at moderate concentrations. The line is given by Eq. [4].

RESULTS

A. Ubbelohde Viscometry

The data from the Ubbelohde viscometry experiments at low concentration are shown in Fig. 3. The straight line shows that these data are within the linear region described by Einstein's expression, i.e., $\eta_r = 1 + 2.5\phi$. The volume fraction $\phi = cq$, where c is the concentration (g/ml) and q is the specific volume. From the slope of the graph $q = 0.92 \pm 0.01$ ml/g. This specific volume is somewhat higher than the values reported previously (1, 2) and suggests the particles are porous. Van Helden *et al.* reported that uncoated silica particles prepared in a similar manner were quite porous, containing many ultramicropores (diameter < 1.2 nm). However, during the high-temperature coating reaction, siloxane bridges form, which can close off the pores and which would explain why the N_2 adsorption did not indicate any porosity. As is seen later, this value of q is consistent with the viscosities found at higher concentrations and so is used to calculate volume fractions hereafter.

Measurements were made with the Ubbe-

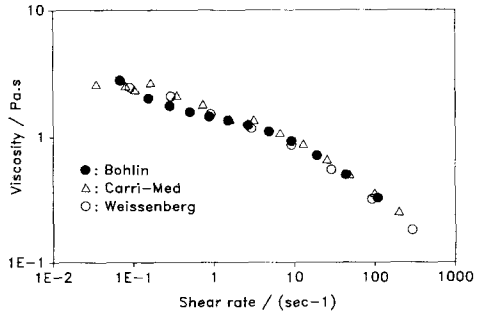

FIG. 5. Comparison of steady shear viscosity for the three instruments: volume fraction is 0.615.

lohde viscometer at volume fractions up to 0.4. It was found that up to $\phi = 0.2$, a cubic expression fitted the data well. Figure 4 shows these results and the best-fit line given by

$$\eta_r = 1 + 2.5\phi + 5.0\phi^2 + 53\phi^3. \quad [4]$$

The second-order term agrees quite well with Batchelor's expression [3]. The agreement with the experimental results of de Kruif *et al.* (1) is also good; they give second- and third-order coefficients of 4 ± 2 and 40 ± 20. The results are entirely consistent with previous theoretical and experimental work and clearly confirm that the particles are behaving as hard spheres in these experiments.

B. Cone and Plate Rheometry: Steady Shear

Generally, very good agreement was found between results from the different instruments as can be seen from Fig. 5 in which viscosity is plotted against shear rate for one sample on all three instruments.

In Figs. 6a and 6b the viscosity is shown as a function of shear rate for a range of high concentration solutions. Both the viscosity and the degree of shear thinning increase dramatically from $\phi = 0.55$ to 0.65. For $\phi < 0.63$ the curves show a low shear Newtonian plateau and can be fitted with the Cross equation (46),

$$\frac{\eta - \eta_\infty}{\eta_0 - \eta_\infty} = \frac{1}{1 + (b\dot{\gamma})^m}, \quad [5]$$

where η_0 is the limiting low shear relative viscosity and η_∞ is the limiting high shear relative viscosity.

Table I gives the results from fitting Eq. [5]; generally the calculated η_∞ was zero because no data were available for the high shear plateau region. However, finite values for η_∞ were calculated for the three highest concentrations. When these were put into Eq. [1], a high shear maximum packing fraction, $\phi_{m\infty}$, of 0.71 was determined. Being an extrapolated parameter this value should be treated with caution but it is interesting to note that De Kruif *et al.* found an identical high shear rate value (1) and equated it with layers sliding over each other in a zig–zag fashion. η_{r0} in Table I is the relative zero shear rate viscosity.

$\dot{\gamma}_c$ is the characteristic shear rate at which $\eta = \eta_\infty + \frac{1}{2}(\eta_0 - \eta_\infty)$, i.e., $\dot{\gamma}_c = 1/b$. A corresponding characteristic Peclet number (P_{ec}) has been calculated for comparison with the data of van der Werff and de Kruif (2). It was

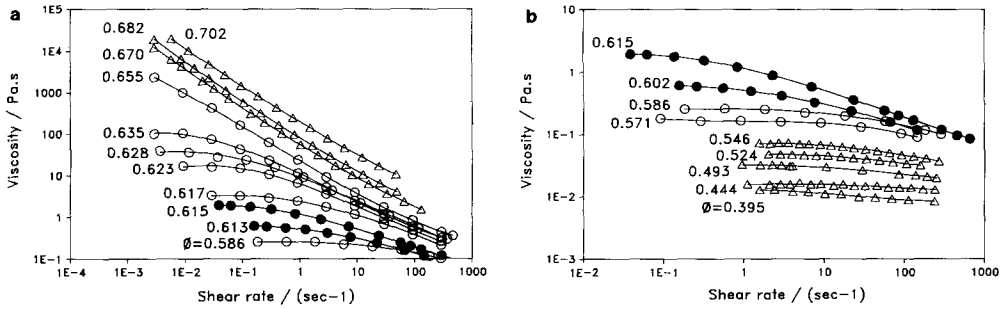

FIG. 6. Steady shear viscosity determined with Carri-Med (△), Weissenberg (○), and Bohlin (●) rheometers: (a) high concentration, (b) medium concentration.

TABLE I

Steady Shear Properties: Cone and Plate Experiments

ϕ	η_0 (Pa s)	η_∞ (Pa s)	η_{r0}	$\dot{\gamma}_c$ (s^{-1})	P_{ec}	m
0.395	0.011		8.0			
0.444	0.016		12			
0.493	0.033		24			
0.524	0.050		36			
0.546	0.075		54	62	7.1×10^{-3}	
0.571	0.17		123	67	7.6×10^{-3}	
0.586	0.26		188	60	6.8×10^{-3}	
0.602	0.62		450	7.0	7.9×10^{-4}	
0.615	2.52		1830	0.68	7.7×10^{-5}	0.50
0.617	3.70		2680	2.2	2.5×10^{-4}	0.60
0.623	19.9	0.09	14400	0.29	3.3×10^{-5}	0.67
0.628	43.4	0.11	31500	0.15	1.7×10^{-5}	0.67
0.635	127	0.125	92030	0.040	4.5×10^{-6}	0.73

found that the Cross equation did not fit the data well for $\phi < 0.55$ due to the lack of data at high Peclet number; thus the parameters in Table I were determined from the graphs of η vs $\dot{\gamma}$, using η_∞ determined from Eq. [1] with $\phi_{m\infty} = 0.71$.

The low shear limiting relative viscosity is shown in Fig. 7a as a function of volume fraction over the whole concentration range. The line plotted is that of Quemada's expression [1] using a ϕ_m of 0.63. There is excellent agreement over the whole concentration range, indicating that Eq. [1] describes hard-sphere behavior up to volume fractions very close to ϕ_m. The zero shear value of ϕ_m agrees exactly with that found previously for hard spheres (1, 2), i.e., 0.63 ± 0.02. This value has been equated with the random dense packing volume fraction (2). There is quite good agreement between the Ubbelohde and cone and plate results. The slight discrepancy is due to shear thinning caused by the relatively high shear rates in the capillary and shows that the Ubbelohde viscometer is not the best instrument to use at higher concentrations. In Fig. 7b the η_{r0} data from this work are compared with data on hard-sphere or near hard-sphere systems from de Kruif *et al.* (1), Mewis *et al.* (7), and Papir and Krieger (47). The agreement is generally very good.

Figure 8a shows the characteristic P_{ec} as a function of volume fraction. Previous workers

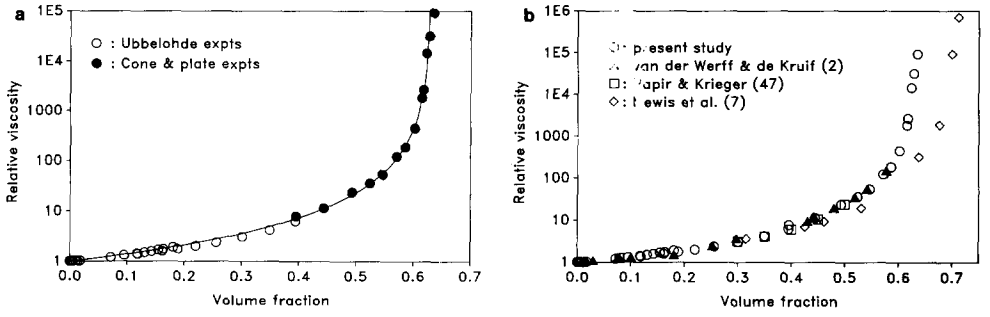

FIG. 7. Low shear rate limiting relative viscosity as a function of volume fraction: (a) compared with Eq. [1], $\phi_m = 0.63$; (b) compared with data from other studies.

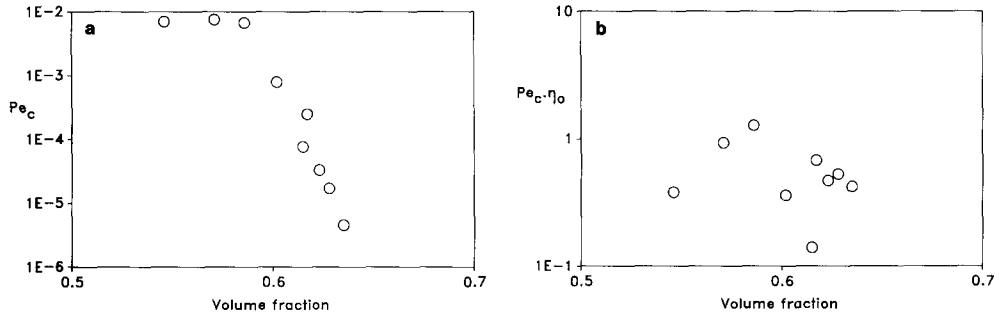

FIG. 8. (a) Characteristic Peclet number as a function of volume fraction. (b) Modified characteristic Peclet number ($P_{ec} \times \eta_0$).

(1) have found that P_{ec} increases as $\phi \rightarrow 0.5$ and then decreases as $\phi \rightarrow \phi_m$. The results here show that P_{ec} decreases rapidly as $\phi \rightarrow \phi_m$ but there is no data for $\phi < 0.5$. The values are similar to those of de Kruif *et al.* but slightly lower. In contrast, plotting $P_{ec} \cdot \eta_0$ vs ϕ gives a very different trend (Fig. 8b). Woods and Krieger (33) suggested a similar parameter but used the suspension viscosity at $\dot{\gamma}_c$ rather than η_0. Presenting the data in this way amplifies the noise but most of the points lie within 0.5 ± 0.2 and there is no clear trend with ϕ. The Peclet number is by definition the balance of Brownian and hydrodynamic forces and thus $P_{ec} \cdot \eta_0$ should be used to express the correct hydrodynamic forces. Thus it appears that shear thinning can be characterized by an effective Peclet number which is independent of concentration. From Table I it can also be seen that the exponent m increases as ϕ increases; that is, the shear thinning becomes more severe as concentration rises.

It is possible to reduce all the data for $\phi < \phi_m$ onto one curve based on the Cross equation, as seen in Figs. 9a and 9b. The superimposition is fair when $b\dot{\gamma}$ is used and excellent when $(b\dot{\gamma})^m$ is used. Thus three parameters (η_0, $\dot{\gamma}_c$, and m) are required to correlate the data for a range of shear rate and volume fraction.

It is widely accepted that at low shear rates, where there is a Newtonian plateau, the suspension microstructure is not significantly perturbed by the shear because the Brownian forces dominate the hydrodynamic forces. Thus the equilibrium structure is restored more rapidly than it is perturbed. In other words the relaxation time is shorter than the reciprocal of the rate of distortion. At higher shear rates the hydrodynamic forces begin to dominate and shear thinning occurs. As the concentration increases, the relaxation time, which is related to the diffusion coefficient of the particles, increases. Thus the shear thin-

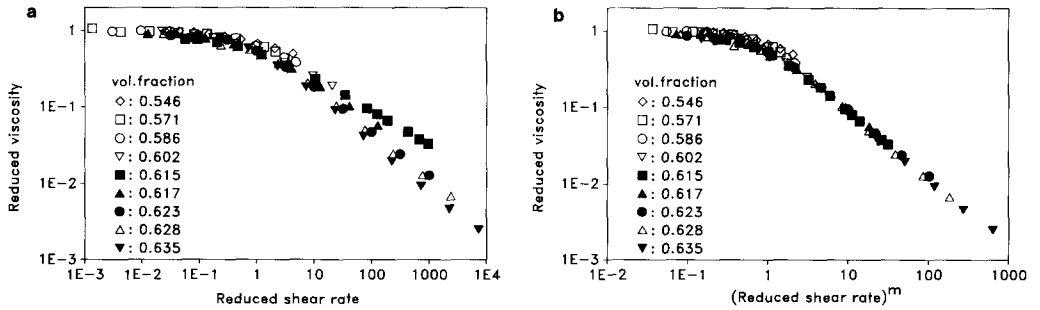

FIG. 9. Reduced viscosity (η/η_0) as a function of reduced shear rate: ($b\dot{\gamma}$) for (a); (b $\dot{\gamma}$) for (b).

ning region shifts to lower shear rates. There have been many interpretations of shear thinning based on the microstructure. It is widely believed (8) that shear thinning is due to ordering of the particles into layers or strings which reduces the energy dissipated under shear. However, Ackerson (12) has recently conducted light-scattering experiments on a sheared hard-sphere system and concluded that a suspension with liquid-like ordering at equilibrium was not ordered in this way at high shear rates (except for evidence of partial string formation at the highest concentrations). The shear thinning was due to a distortion of the liquid-like structure which presumably leads to a decrease in the energy dissipation.

The structure of the suspension in this work is not known. For monodisperse hard spheres a transition from amorphous liquid to crystal-like solid is predicted at $\phi = 0.494$ (48). However, it has been shown (49) that this transition disappears when the polydispersity is greater than 5%. Thus it is likely that in this study the suspensions have a liquid-like structure which is distorted by the shear but without the formation of layers or strings.

Bossis and Brady (50) have studied shear thinning of hard-sphere suspensions by computer simulation and have related the decrease in viscosity to a decrease in the Brownian contribution to the stress due to a small distortion of the microstructure. The increase in the severity of shear thinning with increasing volume fraction, which corresponds to the increase in the exponent m, can also be explained in these terms. At high concentration the contribution to the stress from Brownian forces is greater and thus the decrease in viscosity due to the loss of this contribution will be more marked.

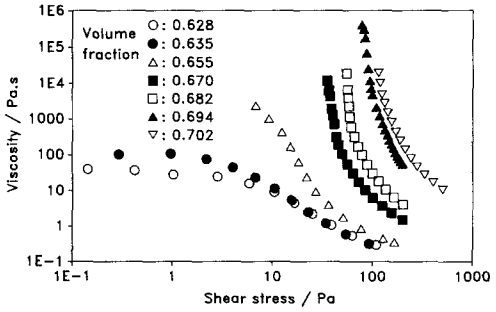

FIG. 10. Viscosity as a function of shear stress for highly concentrated suspensions.

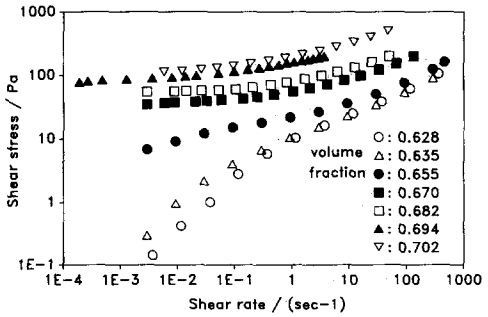

FIG. 11. Shear stress as a function of shear rate for highly concentrated suspensions.

There is a dramatic change in the rheological properties when $\phi > 0.64$, which is clearly seen when viscosity is plotted as a function of shear stress (Fig. 10) or when shear stress is plotted against shear rate (Fig. 11). At low stress the viscosity tends to infinity; that is, there is a yield stress which can be determined by extrapolating to the stress axis in Fig. 11. These values are given in Table II as a function of ϕ and compared with values determined by the vane technique. Due to the small sample size a very small vane had to be used (vane length = 20 mm, diameter = 10 mm). Ideally the measurement should be conducted with vanes of different sizes to allow for end effect

TABLE II

Yield Stress Determined by Vane Technique and Extrapolated from Steady Shear Data

	σ_y (Pa)	
ϕ	Vane	Steady shear
0.670		30 ± 5
0.682	22 ± 5	50 ± 5
0.694	67 ± 6	80 ± 8
0.708	108 ± 2	100 ± 10

corrections. This was not possible in this case but the agreement with the cone and plate determination is quite good nonetheless. As far as the authors are aware this is the first time that a yield stress has been directly measured for a hard-sphere suspension. In many studies on yield stress materials using a vane, it is observed that the stress increases to a maximum value and then falls sharply as the structure is disrupted (51). In contrast, with the hard-sphere suspension the stress reached a maximum and remained steady at that value. This difference reveals much about the type of structure causing the yield stress and the mechanism causing flow. Most yield stress materials consist of an aggregated network of polymer or particles. In order to flow the network must be broken into smaller units which will flow at a lower stress. In a hard-sphere suspension the yield stress is due to dense packing of the particles, flow occurring when the structure is distorted enough to allow particles to move. If σ drops below σ_y the densely packed structure will rapidly reform under Brownian motion and flow will cease. This is discussed more thoroughly in the section on creep experiments. The σ_y results can be fitted to a simple linear equation in ϕ for the concentration range studied,

$$\sigma_y = 1900\phi - 1240. \qquad [6]$$

It should be noted that at these very high concentrations any nonideality in the behavior of the suspension will be amplified. Thus a slight "softness" in the stearyl chain layer would tend to increase the yield stress due to the interaction between the particles. Also, the true volume fraction would be different from that quoted if any solvent is squeezed out from the layer. No scattering experiments have been conducted at such high concentrations to determine the "hardness" of the particles.

Another problem at high concentration could be wall slip in the cone and plate experiment, in which a thin layer of solvent next to one of the surfaces is sheared while the bulk of the sample does not move. However, the smoothness of the steady shear data and the agreement with the vane measurements suggest that wall slip is not significant here.

Tsenoglou (52) has calculated the viscosity of a suspension as a function of shear rate by considering the formation of temporary or permanent clusters. This description is useful in the case where there is no crystal-like ordering. In a hard-sphere suspension it might be envisaged that at concentrations above the low concentration regime particles join their neighbors to form clusters of a temporary nature. The liquid occluded within the cluster does not participate in the flow and thus the effective solid phase concentration is raised causing an increase in viscosity. The degree of clustering increases as volume fraction increases and shear rate decreases, the clusters being broken up by the shear forces leading to shear thinning. Tsenoglou derives semiempirical expressions to calculate the number of particles in the clusters as a function of volume fraction and shear rate. Extending this description it could be conceived that at a certain critical ϕ ($=\phi_m$), a "spanning" cluster forms, filling the available space and resulting in solid-like behavior. This is analogous to gelation of polymers (53) in which cross-linked clusters grow until at the gel point the cluster size becomes infinite. This picture is supported by some computer simulations (54, 55) in which the increase of viscosity with ϕ has been attributed to particle clustering and the viscosity becomes infinite at a percolation-like threshold ϕ_m due to the formation of an infinite cluster.

In all the steady shear experiments conducted no shear thickening or normal stresses were detectable. Due to the small particle size the P_{ec} is relatively low even at quite high shear rates ($P_{ec} = 0.13$ when $\gamma = 1000\ s^{-1}$). Van der Werff and de Kruif (2) using larger particles have attained $P_{ec} = 1200$ and still did not see shear thickening. However, Bossis and Brady (50) have claimed that shear thickening will occur in hard-sphere systems due to clustering but P_{ec} of up to 10^4 are required. Likewise, Barnes (56) has suggested that all suspensions will exhibit shear thickening at high enough shear rate and concentration. In con-

trast, Hoffman (57) claimed that an interparticle interaction of finite range is required as this prevents both free rotation of particles in the layers and motion between the layers. Further experiments with hard spheres at very high P_{ec} are required to resolve the question of shear thickening, although such measurements will not be easy.

Normal stresses have rarely been measured for suspensions. Willey and Macosko (58) reported their presence in suspensions of sterically stabilized latex particles. Computer simulations (54) have predicted that normal stresses only occur when an interparticle interaction exists. The combination of shear and interparticle forces creates an angular dependence in the interaction between particles leading to a normal stress. No such effect is predicted for noninteracting particles. This work on hard spheres supports this prediction.

C. *Cone and Plate Rheometry: Oscillatory Shear*

Dynamic rheological tests were conducted on samples of $\phi > 0.55$. Below this concentration the viscoelastic properties were unmeasurable over the frequency range used (0.03–12 Hz). Every sample was subjected to a strain amplitude sweep at a set frequency to check the linearity of the measurements. Figure 12 shows the results for several concentrations. At a critical amplitude, γ_{crit}, the response becomes nonlinear, causing the storage modulus (G') to decrease, the sharpness of the drop increasing with concentration. γ_{crit} is largest at low concentrations but appears to increase slightly with concentration above $\phi = 0.58$. The values are comparable with those found by Frith *et al.* (6). Below the critical amplitude, in the linear region, energy is not dissipated because the Brownian motion is able to restore the equilibrium structure. Above the critical amplitude the structure is perturbed to a greater extent and energy is dissipated. Ansarifar and Luckham (31) found that the linearity range decreased as the frequency increased and related nonlinearity to shear thinning under steady shear. If this is the case one would expect to see a correlation between $\dot{\gamma}_c$ and γ_{crit}. As we have seen, $\dot{\gamma}_c$ is strongly dependent on ϕ whereas γ_{crit} is not. All oscillatory experiments reported hereafter were conducted at strain amplitudes well within the linear region.

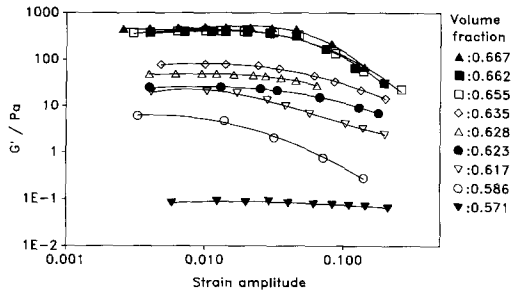

FIG. 12. Storage modulus (G') as a function of strain amplitude, the effect of concentration.

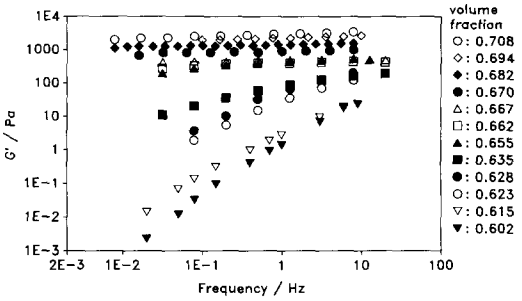

FIG. 13. Storage modulus as a function of frequency, the effect of volume fraction.

In Fig. 13 the storage modulus (G') is shown as a function of frequency for a range of concentrations. At lower concentrations ($\phi < 0.62$) the behavior is that of an inelastic fluid; i.e., G' is quite low and increases rapidly with frequency. At intermediate concentrations ($0.62 < \phi < 0.64$) more pronounced viscoelastic behavior is seen with G' flattening out at high frequencies. At high concentrations ($\phi > 0.64$) elastic solid-like behavior is observed. Here G' is high and almost independent of frequency. The transition from liquid to solid-like behavior occurs over a very narrow concentration range.

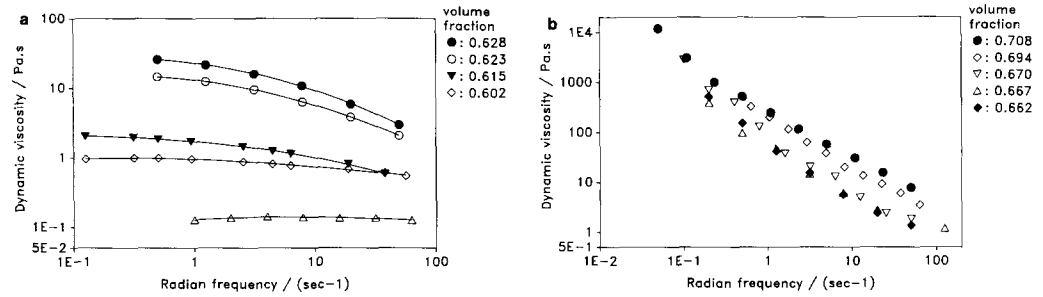

FIG. 14. Dynamic viscosity as a function of frequency: (a) medium concentration, (b) high concentration.

The dynamic viscosity (η') is shown in Figs. 14a and 14b and, as expected, displays trends similar to those of the steady shear viscosity. At low concentrations Newtonian behavior is observed. As the concentration increases, a Newtonian plateau remains at low frequency but shear thinning occurs at higher frequency. The limiting value of the dynamic viscosity at low frequency coincides with the limiting steady shear viscosity at low shear rates, as expected for a simple fluid. However, the correlation disappears at higher rates/frequencies which is not surprising considering the different degrees of microstructure distortion in the two experiments. At high concentrations ($\phi > 0.64$) no Newtonian plateau exists and, as with the steady shear results, the shear thinning occurs across the whole frequency range.

In Fig. 15 the loss tangent (G''/G', where G'' is the loss modulus) is plotted against frequency. This is a very sensitive parameter and shows the transition from liquid-like ($\tan\delta > 1$) to solid-like ($\tan\delta < 1$) behavior.

A characteristic frequency, ω_c, can be determined from where $G' = G''$ (or $\tan\delta = 1$) and is listed in Table III where it is compared with $\dot{\gamma}_c$ from the steady shear tests. There is obviously no direct relationship between the two although the same trends with ϕ are seen. Van der Werff *et al.* (5) have pointed out that in a steady shear experiment the microstructure is perturbed more than with oscillatory shear; thus the particles must diffuse a greater distance to restore the equilibrium state and thus ω_c and $\dot{\gamma}_c$ need not be equal.

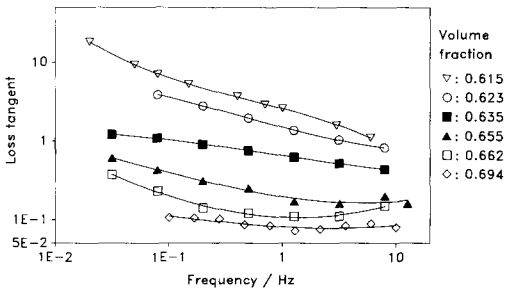

FIG. 15. Loss tangent (G''/G') as a function of frequency.

The results can be understood by considering the relaxation time, τ_r, of the suspension. At low frequencies the experimental time scale $\tau_e > \tau_r$ and the structure is able to relax during the oscillation; thus the suspension behaves as a viscous liquid dissipating most of the energy. As the frequency increases and τ_e approaches τ_r, viscoelastic behavior is observed, the energy being stored and dissipated in similar proportions. At yet higher frequencies $\tau_e < \tau_r$ and the suspension structure is unable to relax; thus most of the energy is stored and the response is elastic. τ_r increases with concentration being effectively infinite when $\phi > \phi_m$, the particles being so closely packed that their

TABLE III

Characteristic Frequency and Shear Rate

ϕ	ω_c (rad·s^{-1})	$\dot{\gamma}_c$ (s^{-1})
0.615	44.5	0.68
0.623	28.9	0.29
0.628	15.7	0.15
0.635	8.41	0.040

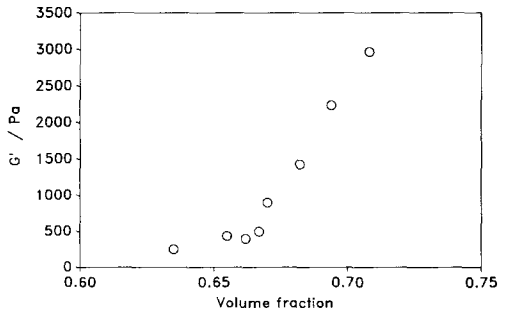

FIG. 16. High-frequency storage modulus as a function of volume fraction.

diffusion is reduced to zero. Under such circumstances $\tau_e < \tau_r$ at all frequencies and solid-like behavior is observed.

In practice most materials have a range of relaxation times associated with different relaxation mechanisms. In a random structure, as expected for the suspension in this study, there would be many different particle environments and the relaxation time of a particle would depend on how crowded it is.

For the higher concentration samples it is possible to determine G'_∞, the limiting high-frequency storage modulus or the elastic modulus which is shown in Fig. 16 as a function of volume fraction. Above $\phi = 0.64$, G'_∞ increases very rapidly with ϕ. G'_∞ is a measure of the suspension's resistance to deformation and thus would presumably be infinite for a close-packed structure at the maximum possible concentration. For a monodisperse suspension this would be the hexagonal close-packed structure at $\phi \approx 0.74$. Goodwin *et al.* (59) observed a much weaker dependence of G'_∞ on ϕ for their charged particles due to the softness of the interparticle interaction.

Measurement of the storage modulus can provide an insight into the normal stresses expected in steady shear flow. Simple fluid theory predicts that

$$\lim_{\omega \to 0} \frac{G'(\omega)}{\omega^2} = \frac{1}{2} \lim_{\dot{\gamma} \to 0} \frac{N_1(\dot{\gamma})}{\dot{\gamma}^2}, \qquad [7]$$

where N_1 is the first normal stress difference. The oscillatory experiments show that G' is finite at low frequency and thus N_1 should also be finite. However, G' is very low at low frequency and the corresponding value of N_1 at low shear rate would be far too low to be detected in the steady shear experiments.

Finally in this section we compare results from the Weissenberg and Bohlin instruments in the oscillatory mode in Fig. 17. The data agree quite well at higher frequencies but the Bohlin values for G' are considerably lower at low frequencies. The stress is constant for the Bohlin and the strain amplitude thus decreases as frequency increases. At low frequencies the strain amplitude will be greater than the critical value, causing the response to be nonlinear and the G' values to be lower than the true linear value.

D. Creep Experiments

Creep tests were conducted using the Bohlin and Carri-Med constant stress instruments. A preset stress was applied and the strain measured as a function of time. In addition, the relaxation when the stress was released was also monitored; this is expressed as a recoverable strain. Three categories of behavior were observed. At lower concentrations ($\phi < 0.6$) the suspensions acted as viscous fluids with strain increasing linearly with time. In this case the recoverable strain was not measurable. As $\phi \to \phi_m$ viscoelastic behavior was observed and a typical example is shown in Fig. 18 in which the strain is plotted against time. At very short times (t < 1 s) the response to the applied

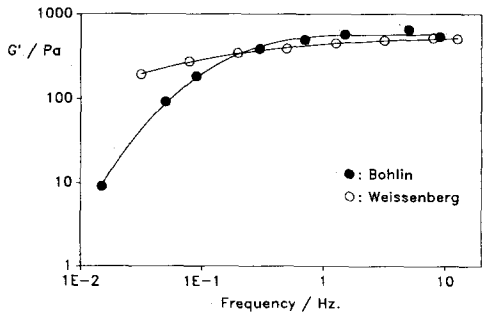

FIG. 17. Comparison of oscillatory data determined using two instruments. $\phi = 0.655$.

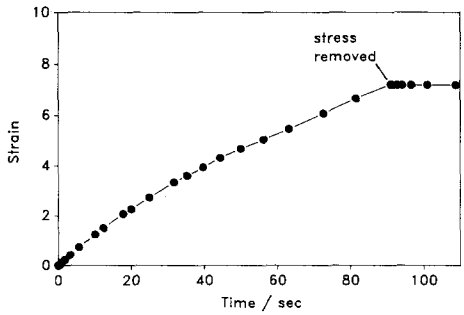

FIG. 18. Creep and recovery strain as a function of time, $\phi = 0.615$, stress = 0.5 Pa.

TABLE IV

Yield Stress from Creep Experiments

ϕ	σ_y (Pa)
0.670	25 ± 5
0.682	45 ± 5
0.694	90 ± 5
0.708	90 ± 10

stress is elastic and if the stress is removed at this stage there is complete recovery of strain. At longer times ($1 \text{ s} < t < 20 \text{ s}$) the response is viscoelastic as the microstructure is increasingly distorted; this is demonstrated by the nonlinear initial section of the curve. At very long times ($t > 40$ s) a steady state is reached and the response is viscous as shown by the linear part of the curve. When this steady state has been achieved the strain recovered on removing the stress is very small. The transition from viscous liquid to viscoelastic behavior occurs smoothly but over a narrow concentration range.

When $\phi > \phi_m$, there is a sudden change in behavior; three characteristic responses were observed depending on the applied stress. At low stresses elastic solid-like behavior was observed as shown in Fig. 19a (σ = 20, 30 Pa). Here the strain rapidly reached a steady value after which no creep occurred. When the stress was released there was almost complete strain recovery, the recoverable strain increasing linearly with applied stress. In principle it is possible to derive G'_∞ from the short time response but this was obscured by the inertia effects of the instrument which caused a decaying oscillation. At higher stress a slow creeping flow occurred but a steady-state viscosity was not achieved and the strain was not fully recovered on release of the stress (Fig. 19b, σ = 40 Pa). At yet higher stresses the sample "yielded" and a steady-state viscosity was attained fairly rapidly. In this region the recoverable strain was independent of stress. The stresses corresponding to this yielding, i.e., at which steady flow is first observed, are listed in Table IV as a function of ϕ. Comparison with Table II shows good agreement with the values extrapolated from the steady shear experiments.

Chen and Zukoski (36) conducted a series of creep tests on ordered, charge-stabilized latex suspensions and observed behavior similar to that seen here. They reported four flow regimes for concentrated systems, with increas-

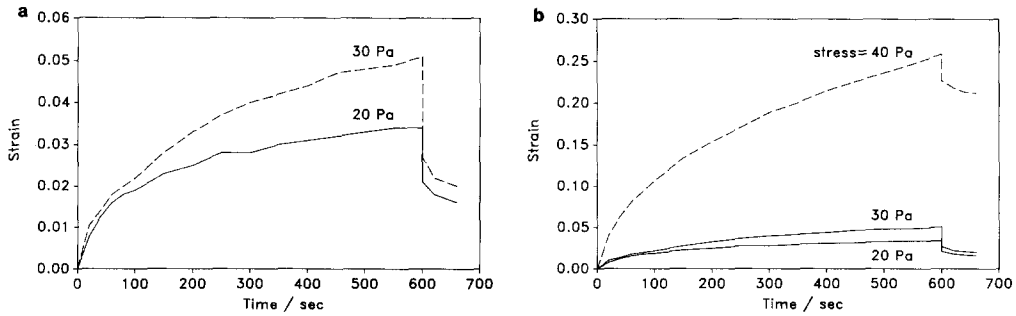

FIG. 19. Creep and recovery strain as a function of time, $\phi = 0.682$: (a) low stress, (b) high stress.

ing stress: (i) elastic solid-like, (ii) elasto-viscous (creeping flow), (iii) low-stress steady flow, and (iv) high-stress steady flow. Systems (iii) and (iv) were separated by an abrupt drop in viscosity which they attributed to a dramatic change in structure. No such change is seen in this work but the first three regimes correlate closely with hard-sphere behavior. Chen and Zukoski interpreted the different flow types as follows. At low stress the structure is strong enough to resist flow and acts as an elastic solid. As stress increases a "defect flow" occurs in which the applied stress biases the interaction potential and the particles diffuse into vacant sites (defects) to relieve the strain. At higher stresses the particles begin to move in a collective manner in which layers move over one another in a zig–zag fashion.

As mentioned before, it is likely that the suspensions in this work have an amorphous structure up to high ϕ. Whether at very high ϕ a crystal-like structure or simply an amorphous glass forms is not known. If there was a crystalline structure present no iridescence would be seen due to the small particle size; X-ray or neutron-scattering experiments would be necessary to elucidate the structure. However, the arguments of Chen and Zukoski can be applied to these suspensions even if they have glass-like structures. At low stress the glass resists flow leading to elastic behavior. It could be argued that being a glass there should be flow at any stress provided it is applied for long enough. This may be true but the same has been stated for all substances (61). On a practical time scale a yield stress was measured and, as the stress increased, a change in flow was observed. It is easy to see how the creeping flow could occur in the glassy state, a stress-biased diffusion of particles with no significant change in structure. As the stress increases further the structure is distorted enough to allow a collective steady-state flow, possibly through an ordering of the particles.

CONCLUSIONS

Theory has yet to fully describe hard-sphere suspension rheology at high concentrations and few experimental studies have probed this region. Results which extend the available experimental knowledge to very high concentrations are presented here. When $\phi < 0.6$ the steady shear rheological properties of this hard-sphere system compare well with those found by other studies on hard spheres. Above $\phi = 0.6$ the steady properties rapidly change with dramatic increases in steady shear viscosity and shear thinning. The response to oscillatory shear also changes markedly, the suspensions becoming viscoelastic with the storage modulus reaching a limiting high frequency value. However, the suspensions still flow under an applied stress. Above ϕ_m (=0.63) an abrupt transition is observed to elastic solid-like behavior. This is characterized by the absence of a low shear Newtonian plateau under steady shear and nearly Hookean elastic behavior under oscillatory shear. In addition, a yield stress has been measured for suspensions at very high concentrations by three different techniques; steady shear, creep, and vane.

ACKNOWLEDGMENTS

We thank the microbiology department of Monash University for the electron microscopy and David Mainwaring for the surface area measurements. The work of D.A.R.J. was supported by Dulux Australia Ltd. and a National Research Fellowship. Work in suspension rheology is now supported by a Special Research Centre Grant from the Australian Research Council.

REFERENCES

1. De Kruif, C. G., van Iersel, E. M. F., Vrij, A., and Russel, W. B., *J. Chem. Phys.* **83,** 4717 (1985).
2. Van der Werff, J. C., and de Kruif, C. G., *J. Rheol.* **33,** 421 (1989).
3. Van der Werff, J. C., de Kruif, C. G., and Dhont, J. K. G., *Physica A* **160,** 205 (1989).
4. Mellema, J., de Kruif, C. G., Blom, C., and Vrij, A., *Rheol. Acta* **26,** 40 (1987).
5. Van der Werff, J. C., de Kruif, C. G., Blom, C., and Mellema, J., *Phys. Rev. A* **39,** 795 (1989).
6. Frith, W. J., Strivens, T. A., and Mewis, J., *J. Colloid Interface Sci.* **139,** 55 (1990).
7. Mewis, J., Frith, W. J., Strivens, T. A., and Russel, W. B., *AIChE J.* **35,** 415 (1989).
8. Hoffman, R. L., *Trans. Soc. Rheol.* **16,** 155 (1972); *J. Colloid Interface Sci.* **46,** 491 (1974).
9. Johnson, S. J., de Kruif, C. G., and May, R. P., *J. Chem. Phys.* **89,** 5909 (1988).

10. Ackerson, B. J., van der Werff, J. C., and de Kruif, C. G., *Phys. Rev. A* **37,** 4819 (1988).
11. Ackerson, B. J., and Pusey, P. N., *Phys. Rev. Lett.* **61,** 103 (1988).
12. Ackerson, B. J., *J. Rheol.* **34,** 553 (1990).
13. Einstein, A., *Ann. Phys.* **19,** 289 (1906).
14. Batchelor, G. K., *J. Fluid Mech.* **83,** 97 (1977).
15. Russel, W. B., and Gast, A. P., *J. Chem. Phys.* **84,** 1815 (1986).
16. Wagner, N. J., and Russel, W. B., *Physica A* **155,** 475 (1989).
17. Beenakker, C. W. J., *Physica A* **128,** 48 (1984).
18. Woodcock, L. V., *Phys. Rev. Lett.* **54,** 1513 (1985).
19. Bossis, G., and Brady, J. F., *J. Chem. Phys.* **80,** 5141 (1984).
20. Heyes, D. M., *J. Non-Newtonian Fluid Mech.* **27,** 47 (1988).
21. Hopkins, A. J., and Woodcock, L. V., *J. Chem. Soc. Farad. Trans.* **86,** 2121 (1990); **86,** 2593 (1990).
22. Evans, D. J., *Int. J. Thermophys.* **7,** 87 (1986).
23. Hess, S., *Int. J. Thermophys.* **6,** 657 (1985).
24. Van Helden, A. K., Jansen, J. W., and Vrij, A., *J. Colloid Interface Sci.* **81,** 354 (1981).
25. Vrij, A., Jansen, J. W., Dhont, J. K. G., Pathmamanoharan, C., Kops-Werkhoven, M. M., and Fijnaut, H. M., *Faraday Discuss. Chem. Soc.* **76,** 19 (1983).
26. Moonen, J., and Vrij, A., *Colloid Polym. Sci.* **266,** 1140 (1988).
27. De Kruif, C. G., Briels, W. J., May, R. P., and Vrij, A., *Langmuir* **4,** 668 (1988).
28. Quemada, D. E., *in* "Advances in Rheology: Vol. 2, Fluids" (B. Mena *et al.,* Eds.). Universidad Nacional Autónama de Mexico, Mexico City, 1984.
29. Krieger, I. M., and Dougherty, T. J., *Trans. Soc. Rheol.* **3,** 137 (1959).
30. Mewis, J., *in* "Proceedings, Xth International Congress on Rheology" (P. H. T. Uhlherr, Ed.), Vol. 1, p. 61, Sydney, 1988.
31. Ansarifar, M. A., and Luckham, P. F., *Colloid Polym. Sci.* **267,** 736 (1989).
32. Tadros, Th. F., and Zsednai, A., *Colloids Surf.* **43,** 95 (1990).
33. Woods, M. E., and Krieger, I. M., *J. Colloid Interface Sci.* **34,** 91 (1970).
34. Russel, W. B., and Benzing, D. W., *J. Colloid Interface Sci.* **83,** 178 (1981).
35. Buscall, R., Goodwin, J. W., Hawkins, M. W., and Ottewill, R. H., *J. Chem. Soc. Faraday Trans. 1* **78,** 2873 (1982).
36. Chen, L-B., and Zukoski, C. F., *J. Chem. Soc. Faraday Trans.* **86,** 2629 (1990).
37. Russel, W. B., and Benzing, D. W., *J. Colloid Interface Sci.* **83,** 163 (1981).
38. Buscall, R., Goodwin, J. W., Hawkins, M. W., and Ottewill, R. H., *J. Chem. Soc. Faraday Trans. 1* **78,** 2889 (1982).
39. Dhont, J. K. G., van der Werff, J. C., and de Kruif, C. G., *Physica A* **160,** 195 (1989).
40. Mellema, J., van der Werff, J. C., Blom, C., and de Kruif, C. G., *Phys. Rev. A* **39,** 3696 (1989).
41. Stöber, W., Fink, A., and Bohn, E., *J. Colloid Interface Sci.* **26,** 62 (1968).
42. White, J., and Jamie, I., personal communication.
43. Wagner, N. J., Fuller, G. G., and Russel, W. B., *J. Chem. Phys.* **89,** 1580 (1988).
44. Jansen, J. W., de Kruif, C. G., and Vrij, A., *J. Colloid Interface Sci.* **114,** 481 (1986).
45. Nguyen, Q. D., and Boger, D. V., *J. Rheol.* **27,** 321 (1983).
46. Cross, M. M., *J. Colloid Sci.* **20,** 417 (1965).
47. Papir, Y. S., and Krieger, I. M., *J. Colloid Interface Sci.* **34,** 126 (1970).
48. Hoover, W. G., and Ree, F. H., *J. Chem. Phys.* **49,** 3609 (1968).
49. McRae, R., and Haymet, A. D. J., *J. Chem. Phys.* **88,** 1114 (1988).
50. Bossis, G., and Brady, J. F., *J. Chem. Phys.* **91,** 1866 (1989).
51. Nguyen, Q. D., and Boger, D. V., *J. Rheol.* **29,** 335 (1985).
52. Tsenoglou, C., *J. Rheol.* **34,** 15 (1990).
53. Vilgis, T. A., and Winter, H. H., *Colloid Polym. Sci.* **266,** 494 (1988).
54. Brady, J. F., and Bossis, G., *J. Fluid Mech.* **155,** 105 (1985).
55. Durlofsky, L. J., and Brady, J. F., *J. Fluid Mech.* **200,** 39 (1989).
56. Barnes, H. A., *J. Rheol.* **33,** 329 (1989).
57. Hoffman, R. L., *Adv. Colloid Interface Sci.* **17,** 161 (1982).
58. Willey, S. J., and Macosko, C. W., *J. Rheol.* **22,** 525 (1978).
59. Goodwin, J. W., Gregory, T., Miles, J. A., and Warren, B. C. H., *J. Colloid Interface Sci.* **97,** 488 (1984).
60. Barnes, H. A., Hutton, J. F., and Walters, K., "An Introduction to Rheology," p. 72. Elsevier, Amsterdam, 1989.
61. Barnes, H. A., and Walters, K., *Rheol. Acta* **24,** 323 (1985).